



Detailed Asian summer monsoon changes during the Mid Holocene and their teleconnections with the northern high latitudes

Bin Zhao^a, Yingfang Cui^{b,*}, Kan Zhao^a, Yongjin Wang^a, Hai Cheng^c, R. Lawrence Edwards^d, Yijia Liang^{a,e,**}

^a School of Geography, Nanjing Normal University, Nanjing, 210023, China

^b Nanjing Institute of Tourism and Hospitality, Nanjing, 210000, China

^c Institute of Global Environmental Change, Xi'an Jiaotong University, 710075, Xi'an, China

^d Department of Earth and Environmental Sciences, University of Minnesota, Minneapolis, MN, 55455, USA

^e College of Geosciences, Nantong University, Nantong, 226000, China

ARTICLE INFO

Handling editor: Dominik Fleitmann

Keywords:

The Holocene
Stalagmite
Asian summer monsoon
Southwestern China

ABSTRACT

The Mid Holocene is a period of warm and optimum climate; however, some geological records reveal a climatic instability during this time interval. In East Asia, the detailed characteristics of monsoonal climate change and associated mechanisms remain debated in the Mid Holocene. Here we reconstruct a high-resolution Asian summer monsoon record based on six $^{230}\text{Th}/\text{U}$ dates and 255 stable isotope measurements ($\delta^{18}\text{O}$ and $\delta^{13}\text{C}$) from a stalagmite in Tiechang Cave, Guizhou Province, China, spanning from ~6.7 to 5.6 ka BP. Both stalagmite TC5 $\delta^{18}\text{O}$ and $\delta^{13}\text{C}$ records detect a monsoon weakening event at around 6.5 ka BP, which is supported by speleothem records in the Asian monsoon domain, indicating its regional significance. This 6.5 ka weak monsoon event corresponds to prominent sea ice expansion and surface cooling in the Barents Sea. The expansion of sea ice coverage inhibited the formation of the North Atlantic Deep Water, weakened the Atlantic Meridional Overturning Circulation (AMOC), and induced widespread hemispheric cooling through the AMOC, which led to the Asian summer monsoon weakening. This weak monsoon interval around 6.5 ka BP is also coherent with a relatively high frequency in the El Niño Southern Oscillation (ENSO) variability, supporting the ENSO-monsoon relationship observed during the Late Holocene. In addition, spectral analyses reveal a significant periodicity of ~60–80 years in TC5 $\delta^{18}\text{O}$ and $\delta^{13}\text{C}$ records, which may reflect the primary modulation of the Asian monsoon by the Atlantic multidecadal variability and the secondary influence of the solar activity (the Gleissberg cycle). Our TC5 $\delta^{18}\text{O}$ and $\delta^{13}\text{C}$ records suggest that a series of multidecadal oscillations, as well as a weak monsoon event, existed in the Asian monsoon region during the relatively warm and optimum Mid Holocene, and are likely associated with climate changes in the North Atlantic.

1. Introduction

The Holocene is the latest interglacial in the Quaternary and has been broadly divided into three time periods: the Early Holocene (~11.6–8.2 ka BP), the Mid Holocene (~8.2–4.2 ka BP), and the Late Holocene (~4.2 ka BP to the Industrial Revolution) (McKay et al., 2024). The Mid Holocene is a period of sustained high summer insolation in the northern hemisphere when the extent of the boreal ice sheet was reduced to a relatively stable stage, and when the climate was warm in the northern high latitudes. It is also referred to as the Holocene Climatic

Optimum, when the wet and warm climate and environmental conditions for human survival are optimal (Ren and Yi, 2019). Therefore, understanding the climate variabilities and mechanisms during the Mid Holocene is important.

The stability of the global climate during the Holocene Climatic Optimum, as an “analog” for the state of the climate in the context of future global warming, has long been a subject of controversy. For example, a large number of climate reconstructions reveal that the Holocene was far from a stable climate pattern, prominently characterized by a series of oscillatory and/or abrupt change events on

* Corresponding author.

** Corresponding author. School of Geography, Nanjing Normal University, Nanjing, 210023, China.

E-mail addresses: cuiyingfang86@163.com (Y. Cui), lucy2012_2015@163.com (Y. Liang).

interdecadal to centennial timescales (Bond et al., 1997, 2001; Fleitmann et al., 2003; Mayewski et al., 2004; Wang et al., 2005; Moros et al., 2006; Isono et al., 2009; Axford et al., 2009; Dixit et al., 2014; Hou et al., 2012; Owen et al., 2016). Among the centennial-scale climate oscillations, the 8.2 ka event received much attention and has been well studied (Alley et al., 1997; Barber et al., 1999; Johnsen et al., 2001; Fleitmann et al., 2003; Alley and Agustsdottir, 2005; McKay et al., 2024). Meanwhile, a series of weak monsoon events occurred in the Asian monsoon region during the Mid Holocene. For instance, Tan et al. (2020) found that the stalagmites from Wuya Cave on the southwestern margin of the Loess Plateau, northern China, with precise U-Th dating (~1 % dating error), clearly recorded Asian monsoon weakening events dated at approximately 5.49 ka BP, corresponding to Bond event 4. In addition, three weak monsoon events centered at around 3.53, 4.90, and 6.26 ka BP were also recorded (Tan et al., 2020). A 5-year-resolution absolute-dated $\delta^{18}\text{O}$ record from Dongge Cave, southern China, provides a continuous history of the Asian summer monsoon over the past 9000 years (Wang et al., 2005). The general trend in the Dongge record is punctuated by eight weak monsoon events, each lasting ~1 to 5 centuries, centered at 0.5, 1.6, 2.7, 4.4, 5.5, 6.3, 7.2, and 8.3 ka BP, with a temporal spacing averaging ~1.2 kyears (Wang et al., 2005). Jo et al. (2017) identified six weak monsoon events through high-resolution oxygen isotope analysis of a stalagmite BN-1 from a cave on the Korean Peninsula, revealing millennial-scale quasi-periodic variations of the East Asian Summer Monsoon since the Mid Holocene, which included a 5.5 ka weak monsoon event.

Studies of various geological records (stalagmites, lake sediments, peat, etc.) in southwestern China shows that the reconstructed records in this region during the Mid Holocene are sensitive to weak monsoon events, consistent with other geological records in the monsoonal regions of China, and the triggering and amplification mechanisms involve multiple processes such as solar activity, sea-air interactions, and atmospheric circulation reorganizations (Zhang et al., 2004; Zhang and Pu, 2011; Wu et al., 2023). Based on the analyses of $\delta^{18}\text{O}$ proxy and sedimentation rate, Zhang and Pu (2011) identified a cold and dry event during the interval of 6.0–5.1 ka BP, corresponding to the “Mid-Yangshao Cold Period”, and a transient cooling event from 4.7 to 4.5 ka BP, and thus revealed that the Mid-Holocene monsoon recession was related to global climatic changes. High-precision $^{230}\text{Th}/\text{U}$ -dated and $\delta^{18}\text{O}$ records of three stalagmites from Xiangshui Cave, Dongge Cave, and Lajia Xianren Cave reveal that the climate conditions during the period of 6–4 ka BP gradually shifted from warm and humid to cold and dry, and that temperatures declined gradually with fluctuations, suggesting a decreasing trend of the Asian summer monsoon (Zhang et al., 2004). Wu et al. (2023) reconstructed the Holocene mean annual atmospheric temperature changes in southwestern China, using the brGDGTs indicator of the Yangzonghai, Yunnan, and found a significant cooling event around 6.5 ka BP, emphasizing the forcing of the greenhouse gases and annual solar radiation in the northern hemisphere. However, using the TRACE-21ka climate model, Zhang et al. (2021) found that, compared with the Early Holocene, the complete melting of the ice sheet in the Mid Holocene and the disappearance of the ice sheet's effect on the westerly wind blocking caused the weakening of the westerly belt oscillations in the mid-latitudes, and through the westerly-monsoon interactions, the variabilities of the Asian monsoon was reduced, resulting in a more stable monsoon climate in the East Asia during the Mid Holocene. Therefore, further studies on monsoonal climate stabilization during the Mid Holocene are necessary, which can provide a background for assessing possible human-environment interactions in the Asian monsoon region under future global warming scenarios.

In this study, we reconstruct an Asian summer monsoon evolution record with an average resolution of 4 years over the period of 6.7–5.6 ka BP based on uranium dating and stable isotope data from a stalagmite in Tiechang Cave, Guizhou Province, southwestern China. We observe a significantly weak monsoon event in the stalagmite $\delta^{18}\text{O}$ and $\delta^{13}\text{C}$

records, which is centered around 6.5 ka BP and roughly corresponds to the 6.8 ka cold event observed in the marine records. The objectives of our study are: (1) to analyze the characteristics of the 6.5 ka event in the Asian monsoon region, and to clarify the spatial and temporal characteristics of the event by comparing high-resolution stalagmite and marine sediment reconstructions, and (2) to identify the instability and cyclic pattern of monsoon climate changes during the Mid Holocene, as well as its causative mechanisms.

2. Materials and methods

Stalagmite sample TC5 was collected from Tiechang Cave ($27^{\circ}26' \text{N}$, $107^{\circ}11' \text{E}$), Guizhou Province, southwestern China. The cave is about 850 m above sea level and developed in the bedrock of Cambrian dolomite. The area is strongly influenced by the Asian monsoon, with a mean annual temperature of 14°C and a mean annual precipitation of about 1000 mm (Fig. 1). Summer precipitation delivered by monsoon from May to September (Ding and Chan, 2005) reaches ~70 % in this region. Sample TC5 is candle-shaped and consists of yellowish and white pure calcite with a total length of 283 mm and a diameter of about 70 mm (Fig. 2). The depth section of 0–256 mm was used in this study due to the presence of a hiatus at 256 mm.

For stable isotope analyses, a total of 255 subsamples were measured at the School of Geography, Nanjing Normal University, using a Finnigan MAT-253 mass spectrometer coupled to a Kiel Carbonate Device. All results were reported in parts per mil (‰) relative to the Vienna Pee Dee Belemnite (VPDB). Repeated analyses performed on an international standard (NBS19) demonstrated long-term reproducibility, with precisions better than 0.06 ‰ for $\delta^{18}\text{O}$ and 0.05 ‰ for $\delta^{13}\text{C}$ at the 1σ level.

Six powdered sub-samples for $^{230}\text{Th}/\text{U}$ dating were obtained by drilling along the stalagmite growth axis using a carbide dental drill. All dating work was performed at the University of Minnesota. The procedure for chemical separation of uranium and thorium was similar to (Edwards et al., 1986/87; Shen et al., 2002). Uranium and thorium isotope solutions were then analyzed using a multi-collector inductively coupled plasma mass spectrometer (MC-ICP-MS) following methods in (Shen et al., 2002; Cheng et al., 2013). All stalagmite ages obtained are in stratigraphic order with 2σ analytical errors.

3. Results

3.1. Chronology for TC5

A total of six ^{230}Th dates were obtained for stalagmite TC5. U and Th isotope concentrations and ratios, as well as the $^{230}\text{Th}/\text{U}$ data, are shown in Table 1. The measured ^{238}U concentrations range from 359.1 ± 0.4 to 632.5 ± 0.8 ppb, and ^{232}Th concentrations range from 295.9 ± 6 to 1560.5 ± 5.6 ppt. The $^{230}\text{Th}/^{232}\text{Th}$ activity ratios are relatively high, leading to small corrections for initial ^{230}Th of less than 31 years. Given the relatively small dating errors (<6 ‰), and the fact that most of the dating data are arranged in stratigraphic order, we used linear interpolation to create a depth-age model for the stalagmite (Fig. 2). The samples were deposited from 6.7 to 5.6 kilo years before present (ka BP), with an average growth rate of ~0.25 mm/yr.

3.2. $\delta^{18}\text{O}$ and $\delta^{13}\text{C}$ sequences

Combined with chronology, we obtained high-resolution stable isotope ($\delta^{18}\text{O}$ and $\delta^{13}\text{C}$) records for stalagmite TC5, with an average temporal resolution of ~4 years. The $\delta^{18}\text{O}$ values of TC5 vary between -9.2 ‰ and -7.8 ‰, with a mean value of -8.5 ‰ and a magnitude of 1.4 ‰, while the $\delta^{13}\text{C}$ values of TC5 vary between -10.1 ‰ and -6.1 ‰, with a mean value of -7.8 ‰ and an amplitude of 4.0 ‰ (Fig. 2). Changes in TC5 $\delta^{18}\text{O}$ and $\delta^{13}\text{C}$ records are isotropic in general trend, and the Pearson correlation between the two is moderately positive ($r =$

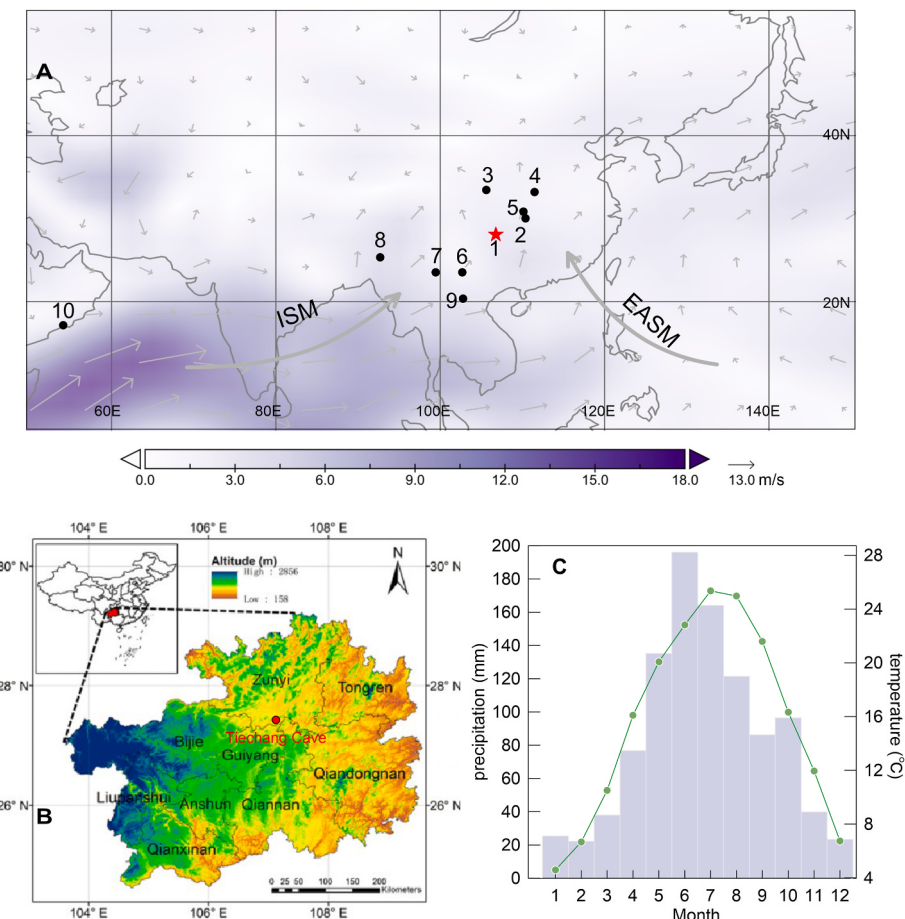


Fig. 1. Geography map and modern climatology of Tiechang Cave. (A) Study region of Tiechang Cave (red star) with other sites (black dots) in the Asian monsoon domain. Tiechang Cave (1, this study), Heshang Cave (2, Hu et al., 2008), Wuya Cave (3, Tan et al., 2020), Dongshiya Cave (4, Zhang et al., 2018), Qingtian Cave (5, Liu et al., 2015), Tengchong Qinghai Lake (6, Zhao et al., 2021), Yangzonghai (7, Wu et al., 2023), Mawmluh Cave (8, Berkelhammer et al., 2013), Tham Doun Mai Cave (9, Griffiths et al., 2020) and Qunf Cave (10, Fleitmann et al., 2007). (B) Topographic map of Guizhou Province, with the location of Tiechang Cave marked red. (C) Monthly mean precipitation (grey bar) and temperature (green lines) at Zunyi station, about 30 km northwest of Tiechang Cave. Grey arrows indicate the Indian summer monsoon (ISM) and the East Asian summer monsoon (EASM), the two subsystems of the Asian summer monsoon. (For interpretation of the references to colour in this figure legend, the reader is referred to the Web version of this article.)

0.51, $p < 0.01$, $n = 255$). The time series of stalagmite $\delta^{18}\text{O}$ revealed that the $\delta^{18}\text{O}$ values of stalagmite TC5 were relatively positive during the period of 6.7–6.4 ka BP, and were oscillating around a background value of $-8.5\text{\textperthousand}$ during the period of 6.4–5.6 ka BP, during which time it fluctuated on centennial to multidecadal timescales. The $\delta^{13}\text{C}$ values of stalagmite TC5 were relatively positive during the period of 6.7–6.4 ka BP, with a mean value of $-7.3\text{\textperthousand}$. After 6.4 ka BP, the $\delta^{13}\text{C}$ profile is superimposed by a series of centennial to multidecadal variations.

4. Discussion

4.1. The 6.5-ka Asian monsoon weakening

The Tiechang Cave stalagmite record has precise U-series dating (error $<6\text{\textperthousand}$) with interannual resolutions, providing a reliable basis for capturing short-timescale climatic events. Our stalagmite $\delta^{18}\text{O}$ record shows the existence of a relatively severe monsoon weakening in the Mid Holocene, roughly centered at 6.5 ka BP, which is therefore referred to as the 6.5 ka event later on (Fig. 3). In the TC5 $\delta^{18}\text{O}$ record, the 6.5 ka event is characterized by an overall U-shaped structure, which is mainly divided into three phases, manifested as a rapid onset, an internal stable phase, and a rapid end. Between 6.7 and 6.6 ka BP, the $\delta^{18}\text{O}$ values underwent a rapid positive deviation (from -9.1 to $-8.1\text{\textperthousand}$) with an amplitude of $\sim 1\text{\textperthousand}$. Thereafter, the $\delta^{18}\text{O}$ values fluctuated above and

below the mean value of $-8.2\text{\textperthousand}$, accompanied by large oscillations on interdecadal to multi-decadal timescales for about 200 years until 6.4 ka BP, when the $\delta^{18}\text{O}$ value was rapidly negatively shifted to a value of $\sim -9.0\text{\textperthousand}$.

In order to test the representativeness of the $\delta^{18}\text{O}$ stalagmite record from Tiechang Cave for the 6.5 ka BP event, we compare our reconstruction with stalagmite records from the Asian monsoon region. Some high-resolution and well-dated stalagmite records clearly capture the 6.5 ka event. For instance, in China, the 6.5 ka event was captured by stalagmite $\delta^{18}\text{O}$ records from Wuya Cave (Tan et al., 2020), Dongshiya Cave (Zhang et al., 2018), Qingtian Cave (Liu et al., 2015), and Heshang Cave (Hu et al., 2008), all characterized with a sharp and positive valley denoted by black arrows (Fig. 3A–D), which may reflect the response of the Asian monsoon to the same climatic forcing. The 6.5 ka event in Wuya, Dongshiya and Qingtian caves lasts 100–200 years, shorter than the duration recorded in the TC5 record. Despite the low temporal resolution of the stalagmite record from Heshang Cave (Fig. 3D), the 6.5 ka event in this record can be clearly identified and exhibits the same amplitude ($\sim 1\text{\textperthousand}$) as in the TC5 stalagmite record. In addition, the MG-1 $\delta^{18}\text{O}$ record from Magou Cave, Henan Province, identifies 14 weak monsoon intervals, including a 6.5 ka event (Cai et al., 2021). In northeast India, the $\delta^{18}\text{O}$ record from Mawmluh Cave (Berkelhammer et al., 2013) shows strong similarity with the TC5 $\delta^{18}\text{O}$ record in terms of the duration (~ 300 years) and the amplitude ($\sim 1\text{\textperthousand}$) in shifts. Besides,

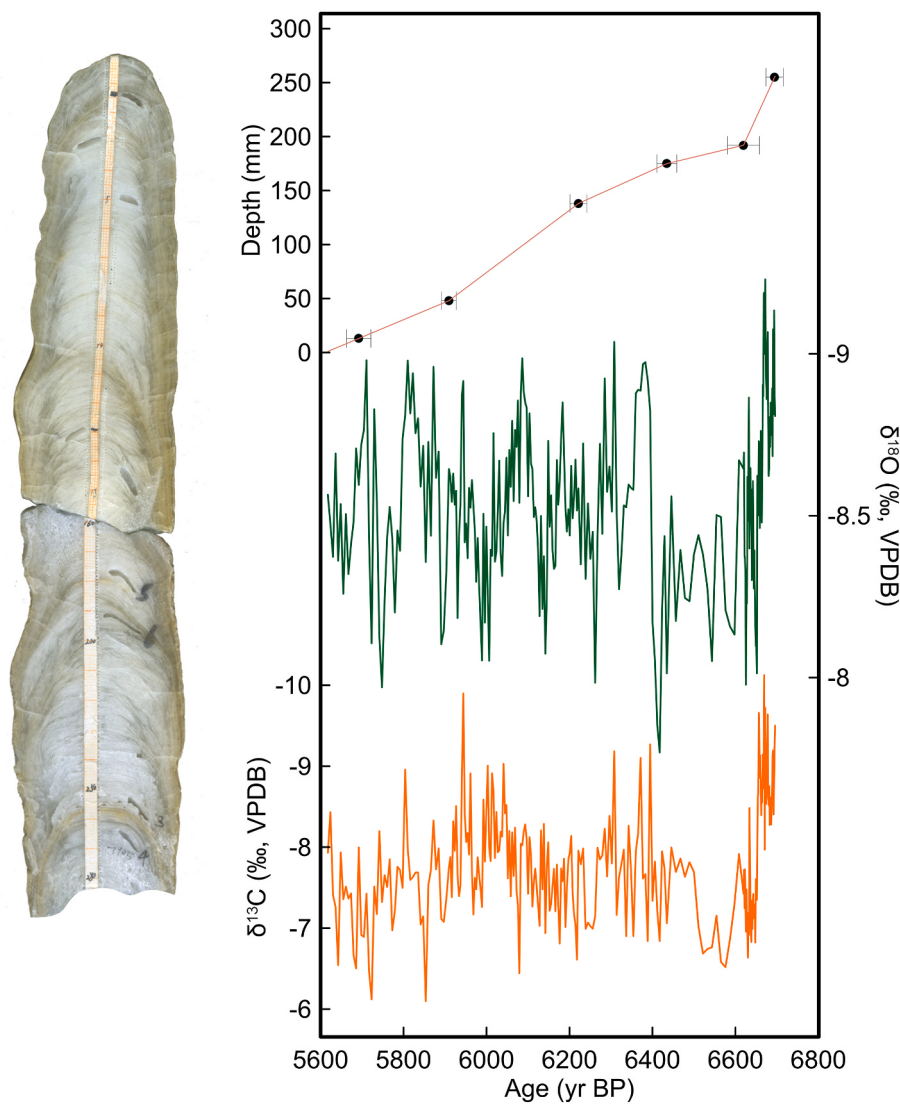


Fig. 2. Sample profile of TC5 (left panel). Chronology and the $\delta^{18}\text{O}$ (green) and $\delta^{13}\text{C}$ (orange) records of TC5 (right panel). Black dots and error bars indicate $^{230}\text{Th}/\text{U}$ age and dating errors. (For interpretation of the references to colour in this figure legend, the reader is referred to the Web version of this article.)

in Southeast Asia, the $\delta^{18}\text{O}$ and $\delta^{13}\text{C}$ records from Tham Doun Mai Cave (Griffiths et al., 2020) (Fig. 3H) also capture the 6.5 ka event. In Oman, this event is also corroborated in the $\delta^{18}\text{O}$ record from Qunf Cave, which shows a weak Indian summer monsoon at around 6.4 ka BP, and is nearly consistent with the 6.5 ka event within dating uncertainties of ~100 years (Fleitmann et al., 2003). Although changes before 6.7 ka BP are scarce from TC5 record due to the limitation of the deposition interval, other speleothem records show that the Asian monsoon was relatively strong and that the onset of this event should be consistently rapid in the Asian monsoon domain. Using high-resolution (3–20 yr) oxygen and carbon isotope records of a stalagmite from the Soreq Cave in Israel, Bar-Matthews and Ayalon (2011) reconstructed palaeoclimatic conditions in the eastern Mediterranean region during the Mid Holocene and identified several interdecadal to centennial-scale climatic events, including the 6.5 ka event.

The TC5 $\delta^{13}\text{C}$ record can help us better understand the monsoon weakening event around 6.5 ka BP. Cave stalagmite $\delta^{13}\text{C}$ is complexly influenced by external conditions (e.g., climate, vegetation, etc.) and depositional processes (e.g., cave ventilation, prior calcite precipitation, etc.), and thus can provide important information on climate and environmental change (Fairchild et al., 2006; Fohlmeister et al., 2020; McDermott, 2004). In principle, the carbon isotope composition of

stalagmites is mainly derived from the composition of soil gas CO_2 , involving biological processes (e.g., plant root respiration, microbial oxidation of organic residues, etc.), vegetation type (C3 or C4 plants), biomass production, and soil respiration (Cerling, 1984; Fairchild et al., 2006; Genty et al., 2003; Lechleitner et al., 2021; McDermott, 2004). The soil gas CO_2 is then dissolved in percolating water and transferred into the cave, depositing on the speleothem. In general, in wet and warm climates, increased biological productivity due to high vegetation coverage and microbial activity leads to higher ^{12}C -rich CO_2 concentrations in the soil (Genty et al., 2003; Fohlmeister et al., 2020). Subsequently, ^{12}C -rich CO_2 is transferred and deposited into secondary carbonate calcite, resulting in the formation of low-value calcite $\delta^{13}\text{C}$. In C3 vegetation dominated regions, $\delta^{13}\text{C}$ values in secondary carbonates typically range from -14 ‰ to -6 ‰, while the calcite $\delta^{13}\text{C}$ values range from -6 ‰ to +2 ‰ in C4 plant dominated regions (McDermott, 2004). At our study site, the average of $\delta^{13}\text{C}$ is -7.8 ‰. Considering the fact that the present vegetation type is mainly composed of C3 forests, we suggest that $\delta^{13}\text{C}$ changes in TC5 should primarily reflect changes in the density of vegetation cover and biomass production (Baldini et al., 2005). Furthermore, previous studies in the Asian monsoon region show strong in-phase coupling of $\delta^{13}\text{C}$ and $\delta^{18}\text{O}$ on the centennial to millennial timescales, and amplitudes in $\delta^{13}\text{C}$ records are often larger than those in

Table 1
230-Th/U dating results for stalagmite TC5 from Tiechang Cave.

Sample Number	238U		232Th		230Th/232Th		δ234U ^a		230Th/238U		230Th Age (yr)		230Th Age (yr BP)	
	(ppb)	(ppt)		(atomic x10 ⁻⁶)		(measured)	(activity)		(uncorrected)	(corrected)		(uncorrected)	(corrected)	
TC5-13	359.1	±0.4	1356.3	±4.8	778.1	±4.1	2429	±4	0.1782	±0.00075	5787	±26	2468	±4
TC5-48	384.1	±0.7	295.9	±6.0	2429.5	±3.8	3942	±81	0.1842	±0.00047	5982	±17	5909	±4
TC5-138	505.5	±0.6	919.9	±5.1	1755.9	±10.7	2430	±4	0.1938	±0.00053	6301	±19	6221	±20
TC5-175	511.1	±0.7	1069.7	±5.1	1577.1	±8.8	2429	±4	0.2002	±0.00063	6517	±23	6435	±24
TC5-192	385.6	±0.7	1560.5	±5.6	841.0	±4.6	2433	±8	0.2064	±0.00093	6716	±35	6619	±38
TC5-255	632.5	±0.8	608.2	±5.6	3560.4	±34.0	2427	±4	0.2076	±0.00055	6768	±20	6694	±21

^a $\delta^{234}\text{U} = ([^{234}\text{U}/^{238}\text{U}]_{\text{activity}} - 1) \times 1000$.

^b $\delta^{234}\text{U}_{\text{initial}}$ was calculated based on 230Th age (T), i.e. $\delta^{234}\text{U}_{\text{initial}} = \delta^{234}\text{U}_{\text{measured}} \times e^{\lambda_{234}\text{T}}$. U decay constants: $\lambda_{238} = 1.55125 \times 10^{-10} \text{ yr}^{-1}$ (Jaffey et al., 1971) and $\lambda_{234} = 2.82206 \times 10^{-6} \text{ yr}^{-1}$ (Cheng et al., 2013). Th decay constant: $\lambda_{230} = 9.1705 \times 10^{-6} \text{ yr}^{-1}$ (Cheng et al., 2013).

^c Corrected 230-Th ages assume the initial 230Th/232Th atomic ratio of $(4.4 \pm 2.2) \times 10^{-6}$. Those are the values for a material at secular equilibrium, with the bulk earth 232Th/238U value of 3.8. Errors are 2σ analytical errors. All ages are corrected to 'present' which is defined as the year 1950 AD.

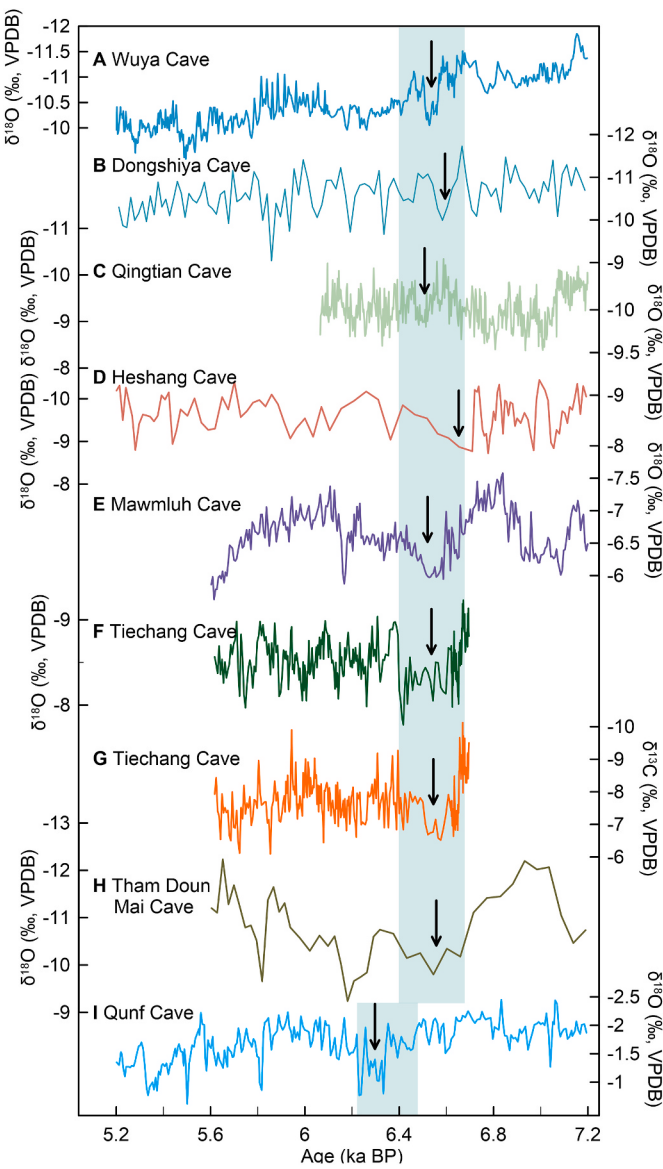


Fig. 3. Comparison of TC5 with other cave stalagmite $\delta^{18}\text{O}$ records in the Asian monsoon domain. The calcite $\delta^{18}\text{O}$ records from (A) Wuya Cave (Tan et al., 2020), (B) Dongshiya Cave (Zhang et al., 2018), (C) Qingtian Cave (Liu et al., 2015), (D) Heshang Cave (Hu et al., 2008), (E) Mawmluh Cave (Berkelhammer et al., 2013), (F) Tiechang Cave (this study), (I) Qunf Cave (Fleitmann et al., 2007). The calcite $\delta^{13}\text{C}$ records from (G) Tiechang Cave and (H) Tham Doun Mai Cave (Griffiths et al., 2020). Green bar and black arrows indicate the 6.5 ka weak monsoon event. (For interpretation of the references to colour in this figure legend, the reader is referred to the Web version of this article.)

$\delta^{18}\text{O}$ records due to the amplification effect of the ecosystem (Zhao et al., 2016; Feng et al., 2020; Liang et al., 2022). In the TC5 records, $\delta^{13}\text{C}$ values and $\delta^{18}\text{O}$ values show similar characteristics during the 6.5 ka BP event, with a relatively positive bias from 6.7 to 6.4 ka BP lasting for ~300 years. The covariation of TC5 $\delta^{13}\text{C}$ and $\delta^{18}\text{O}$ suggests that changes in the local ecosystem and biomass production are tightly associated with soil humidity balance that is controlled by regional hydrological circulation and atmospheric circulation. A similar phenomenon has also been detected in the multi-proxy speleothem records from southwestern China (Feng et al., 2020), in which they interpret the 7.2 ka event as a drought event. The positive bias in TC5 $\delta^{13}\text{C}$ values during the 6.5 ka event reveals the deterioration of the environmental conditions near the cave site, perhaps including decreases in soil humidity, soil respiration, and biomass production, which is closely associated with regional

hydrological changes that is demonstrated by stalagmite $\delta^{18}\text{O}$ record (McDermott, 2004; Fairchild et al., 2006; Zhao et al., 2016).

4.2. Mechanism for the 6.5 ka event in the Asian monsoon domain

The 6.5 ka event captured by the TC5 stalagmite record may be associated with abrupt climate changes in the North Atlantic and the northern high latitudes. Telesiński et al. (2024) used marine records from the Nordic Sea and provided the first detailed description of a cold event centered at 6.8 ka BP, revealing that cold snaps could occur even during this relatively warm Mid Holocene period and that the resulting environmental change could propagate globally. Planktonic foraminifer abundance in both the JM10-330 (Consolario et al., 2018) and MD17730-4 (Telesiński et al., 2015) cores shows low values during 7 and 6 ka BP (Fig. 4A), suggesting low temperatures in the North Atlantic. Ice-raided debris fluxes at the site of MSM5/5–712 (Werner et al., 2013) were significantly increased during that period (Fig. 4B), further

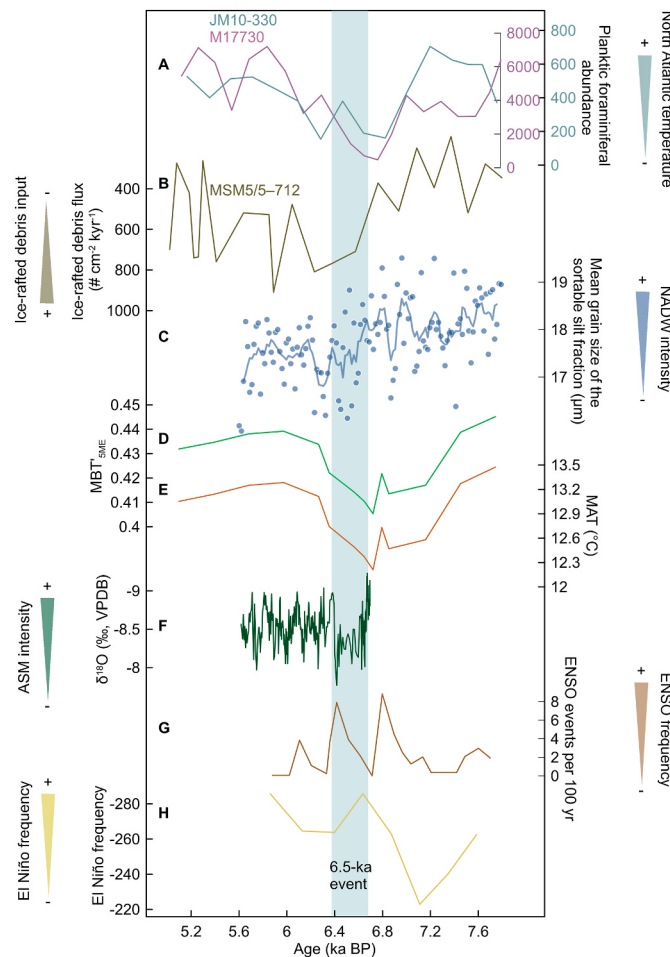


Fig. 4. Comparison of geologic records surrounding the 6.5 ka event. (A) Planktonic foraminifer abundance in cores JM10-330 (ocean green; Consolario et al., 2018) and M17730 (dusty plum; Telesiński et al., 2015). (B) Ice raft debris flux in the MSM5/5–712 core (Werner et al., 2013). (C) North Atlantic Deep Water (NADW) intensity recorded by the mean grain size of the sortable silt fraction in North Atlantic core MD2251 (Hoogakker et al., 2011). (D) The brGDGTs proxy and the inferred Holoocene temperature anomalies in Yangzonghai, Yunnan Province (Wu et al., 2023). (E) Mean annual temperature (MAT) variations at Qinghai Lake, Tengchong, Yunnan Province (Zhao et al., 2021). (F) The $\delta^{18}\text{O}$ record of Tiechang Cave. (G) The number of ENSO events in 100-yr overlapping windows (Moy et al., 2002). (H) El Niño frequency (Zhang et al., 2014). The green bar indicates the 6.5 ka event. (For interpretation of the references to colour in this figure legend, the reader is referred to the Web version of this article.)

suggesting the enhanced influence of the Arctic waters. Within dating errors, the starting point of the 6.5 ka BP event in the Tiechang Cave stalagmite record can be traced to a significant cooling of the subpolar waters in the North Atlantic and the influx of the ice-raided debris (Fig. 4A and B), which may have been caused by the enhanced deep convection in the Greenland Sea and the westward movement of the North Atlantic Deep Water (NADW) current. This significant cooling of the subpolar waters also led to the transport of sea ice from the Barents Sea into the East Greenland Strait, and inhibited the formation of NADW, which then weakened the Atlantic horizontal circulation and perturbed the thermohaline circulation in the eastern Nordic Sea (Telesiński et al., 2024). The decrease in the flow speed of the NADW is evidenced by the mean grain size of the sortable silt fraction for MD2251 (Hoogakker et al., 2011), which started at around 6.6 ka BP and ended at approximately 6.2 ka BP (Fig. 4C).

The reconstruction of multiple proxy-derived sea surface temperature records also implies that the North Atlantic was relatively cold at approximately 6.5 ka BP (Ayache et al., 2018). The cold perturbations in the North Atlantic could propagate through the ocean circulation, which in turn caused widespread hemispheric cooling, documented in records summarized by Wanner et al. (2011). Besides, climate simulations (e.g., TRACE-21ka) show that the intensification of freshwater input and the reduction of surface seawater salinity during the 6.8 ka event weaken the strength of the AMOC and the Atlantic trans-equatorial heat transport, directly affecting the global heat distribution and resulting in a heat deficit in the northern hemisphere at high latitudes, in contrast to a heat surplus in the tropics (Telesiński et al., 2024). The redistribution of heat forces a shift of the Intertropical Convergence Zone (ITCZ) toward the equator in response to changes in the trans-equatorial energy gradient. As noted in previous modeling studies (Sun et al., 2012; Liu et al., 2017, 2020), perturbations in the AMOC could result in a series of climate responses: significant cooling in and around the northern North Atlantic, the deceleration of the AMOC, reorganizations of the Asian monsoon system and a southward shift of the ITCZ. The southward shift of the ITCZ will generally cause a decrease in precipitation north of the equator and an increase in precipitation south of it (Liu et al., 2017, 2020). This shift in precipitation is particularly pronounced in the Atlantic sector. Titanium concentration record from the Cariaco Basin shows a southward movement of the ITCZ and the associated rainfall belt in the tropical Atlantic Ocean at around 6.4 ka BP (Haug et al., 2001), consistent with the Asian summer monsoon weakening (Fig. 4F) within dating errors.

The 6.5 ka event is further evident in other proxy reconstructions in both hemispheres. For example, Wanner et al. (2011) analyzed six cold relapses during the past 10,000 years based on carefully-selected temperature and humidity/precipitation time series, as well as a reconstruction of the glacier advances and retreats, and found one definite cold event occurring between 6.4 and 6.2 ka BP during the Holocene Climate Optimum. They suggested that this cold spell at around 6.4 ka BP interrupted the stable and warm Holocene at least in the northern hemisphere extra-tropical area, and showed that prominent cooling occurred in North America, Africa, central Asia, and northern South America, while a few sites display a warming trend (Wanner et al., 2011). Similarly, Viau et al. (2006) quantified temperature changes over the last 14,000 years based on reconstructions of July mean continental temperatures from pollen records in North America, with a clear cold event occurring around 6.5 ka BP. Lake records in southwestern China are sensitive to this cold event, and the reconstructed mean annual temperature changes based on brGDGTs from Yangzonghai and Tengchong Qinghai lakes in Yunnan reveal that a significant cooling event occurred around 6.5 ka BP (Wu et al., 2023; Zhao et al., 2021) (Fig. 4D and E). Other evidence also suggests that the cooling of the North Atlantic region and the southward shift of the ITCZ during 6.5 and 5.9 ka BP may have contributed to the weakening of the Southeast Asian monsoon (Berkelhammer et al., 2013; Xiao et al., 2009). In addition, the record of West African eolian dust supply at the Site 658C shows that

before the abrupt termination of the African Humid Period at around 5.5 ka BP, the terrigenous dust also increased 10 % at around 6.5 ka BP (deMenocal et al., 2000). Studies show that changes in Saharan vegetation directly affect surface albedo and dust emissions in the Sahara, which in turn affects global temperature change and hence atmospheric circulation and precipitation (Evan et al., 2016; Lu et al., 2025). Climate simulations show that Saharan vegetation deterioration can lead to cooling in the Arctic and Tibetan Plateau: cooling in the Arctic drives a southward shift of the westerly wind belt, and the associated atmospheric wave train propagates eastward, affecting summer monsoon and precipitation in China (Lu et al., 2025). Meanwhile, as the heat source driving the Asian summer monsoon, the cooling of the Tibetan Plateau directly reduces the sea-land thermal gradient, thus weakening the Asian summer monsoon circulation and reducing the Asian summer monsoon precipitation (Lu et al., 2025). The TC5 stalagmite $\delta^{18}\text{O}$ record shows (Fig. 4F) that the oxygen isotopes of Asian monsoon precipitation were significantly positively-biased during the 6.5 ka event, suggesting a systematic recession of monsoon circulation dynamics, possibly also sensitively responding to North Atlantic cooling via the processes of the Saharan vegetation degradation.

Another possible cause for the monsoon weakening in the Asian region might be related to the El Niño frequency and the El Niño Southern Oscillation (ENSO) variabilities during the Mid Holocene. Previously, using the comparison between N1 isotopic data and ENSO proxies, Zhao et al. (2016) found that negative $\delta^{13}\text{C}$ and $\delta^{18}\text{O}$ values during the Late Holocene were consistent with low frequencies in ENSO, and positive $\delta^{13}\text{C}$ and $\delta^{18}\text{O}$ values were coherent with high frequencies in ENSO. We here observe that at around 6.5 ka BP, when the Asian summer monsoon weakened and the biomass production decreased, the frequencies of ENSO and El Niño events increased, further validating the ENSO-monsoon correlation during the Mid Holocene revealed by Zhao

et al. (2016). Such relationship between ENSO and monsoon could be related to the intensity and location of the western North Pacific subtropical high (WPSH) (Tan, 2014; Zhao et al., 2016). During frequent El Niño periods, the Walker circulation weakens, and the WPSH strengthens and stretches westward to southwestern China (Tan, 2014), leading to enriched ^{18}O components in rainfall and decreased precipitation amount in the Asian monsoon region. Besides, impacts of climate changes in the North Atlantic can be transmitted to the Asian monsoon region via the ENSO, although the North Atlantic influence might be limited on the ENSO-monsoon relationship (Wang et al., 2024). Overall, we suggest that abrupt climate changes in the North Atlantic should be the primary forcing for the 6.5 ka Asian monsoon weakening, while the ENSO might exert a potential influence.

4.3. Periodic analysis of Asian summer monsoon variabilities during the mid Holocene

Wavelet analysis reveals significant cycles of ~60–80 years in the TC5 $\delta^{13}\text{C}$ record (Fig. 5A) and significant cycles of ~30, ~60 and ~120 years in the $\delta^{18}\text{O}$ record of TC5 (Fig. 5B). Cross-spectral analysis of the Tiechang Cave $\delta^{18}\text{O}$ and $\delta^{13}\text{C}$ records revealed significant and consistent ~60–80-year cycles, which further supports the strong coupling of the Asian summer monsoon with biomass production/soil humidity on multidecadal timescales (Fig. 5C). In previous studies, the ~60-year cycles have been observed in stalagmites growing during the Late Holocene (Wang et al., 2025), the Last Interglacial Period (Wang et al., 2020) and the early last deglaciation (Liang et al., 2024), indicating the prevalence of this periodicity in the Asian monsoon region.

The ~60–80-year cyclicity in the Asian summer monsoon is highly consistent with the quasi-60-year oscillation of the Atlantic multidecadal variability (AMV) or the Atlantic multidecadal oscillation

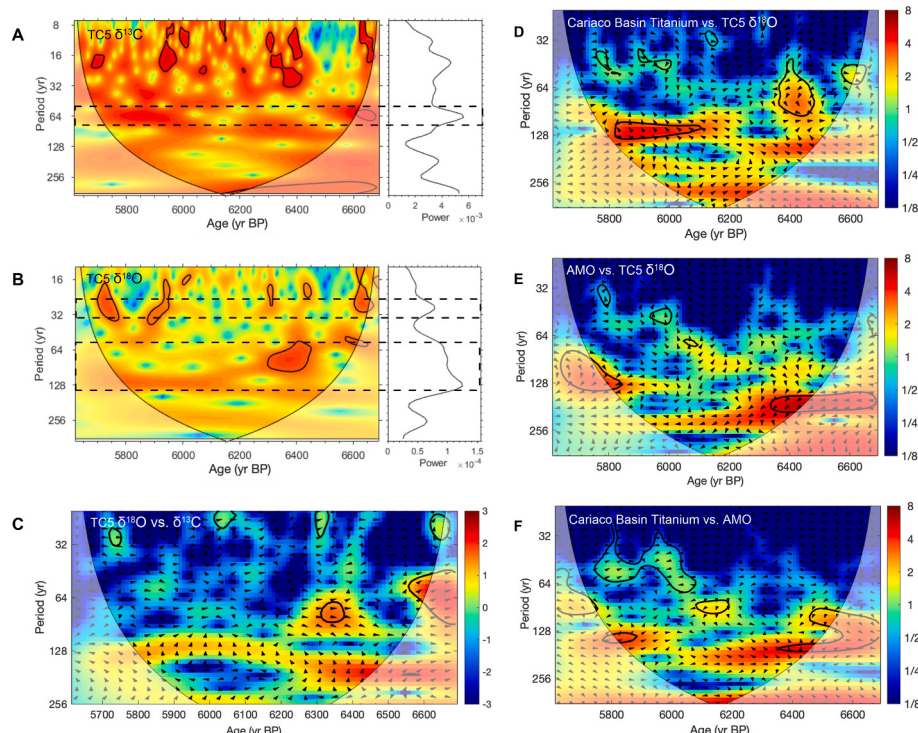


Fig. 5. Cyclicity analyses. (A) Wavelet analysis of the TC5 $\delta^{13}\text{C}$ record. (B) Wavelet analysis of the TC5 $\delta^{18}\text{O}$ record. Cross-spectrum analyses of (C) TC5 $\delta^{18}\text{O}$ and $\delta^{13}\text{C}$ records, (D) TC5 $\delta^{18}\text{O}$ record and Cariaco Basin Titanium content (Haug et al., 2001), (E) TC5 $\delta^{18}\text{O}$ record and AMO index (Zhang et al., 2016), (F) Cariaco Basin Titanium content (Haug et al., 2001) and AMO index (Zhang et al., 2016). Black dashed rectangles in A and B indicate the prominent cyclicities in TC5 $\delta^{18}\text{O}$ and $\delta^{13}\text{C}$ records. The 95 % significance level against red noise is shown by the thick solid line. The spectra were estimated using the method of Grinsted et al. (2004) (<http://nrc.ac.uk/usingscience/crosswavelet-wavelet-coherence>). (For interpretation of the references to colour in this figure legend, the reader is referred to the Web version of this article.)

(AMO), and the Gleissberg cycle (~88 years) in solar activities. The AMV/AMO is a basin-scale mode of sea surface temperature (SST) variability in the North Atlantic with global impacts. As early as in the 1960s, Bjerknes (1964) suggested that the North Atlantic SST was characterized by multi-decadal variability based on observational data. Later, Schlesinger and Ramankutty (1994) demonstrated that there was indeed a 50–88-year oscillation cycle in the North Atlantic SST by analyzing the spectral analysis of global SST data since 1850. Recently, using the long-term output of CMIP5 and CMIP6 models, Li et al. (2025) found that, under global warming, the dominant cycle of the AMV shifted from 10–30 years to 40–60 years. Knudsen et al. (2011) showed that the quasi-persistent ~55–70-year AMO signals featured the North Atlantic ocean-atmosphere variability over the past 8000 years, and they also found that the Gleissberg cycle (~88 years) was prominent during the Mid Holocene. The Gleissberg cycle (Gleissberg, 1965) can be directly linked to the cyclic activity of sunspot formation, and is persistent during the last 12,000 years, according to the record of atmospheric ^{14}C abundance (Peristykh and Damon, 2003).

We compare the high-resolution AMO index record estimated from the KCM HT simulation (Zhang et al., 2016) (Fig. 6A) with the TC5 $\delta^{18}\text{O}$ record (Fig. 6D). Each strong monsoon interval can be well related to the positive phases or peaks of the AMO. This AMO-monsoon relationship is consistent with Fan et al. (2024)'s research, in which they derived a second principal component from the compiled Chinese stalagmite $\delta^{18}\text{O}$ records that could be well matched with North Atlantic SST on the centennial to millennial timescales during the Holocene, supporting the impacts of the AMO on the Asian summer monsoon. The Titanium content of sediments in the Cariaco Basin (Haug et al., 2001) (Fig. 6C), which can be used to track the changes in the AMO (Knudsen et al., 2011) while itself is a proxy for the migration of ITCZ, also shows strong similarity to our Tiechang $\delta^{18}\text{O}$ record on the multidecadal to centennial timescale, especially the peak-to-peak correspondence. We then did cross-spectral analysis on TC5 $\delta^{18}\text{O}$ record, AMO index and Cariaco Basin Titanium record (Fig. 5D, E and F), and found good consistency on the multi-decadal to centennial timescales in each pair, further validating the tight relationship among these records. Furthermore, in the

Cariaco Basin Titanium record, the Gleissberg cycle is prominent from 6800 to 5500 yr BP (Knudsen et al., 2011). We compare both the Titanium record and the TC5 $\delta^{18}\text{O}$ record with the cosmic radiation which is derived based on the first principal component of several radionuclide records (Steinhilber et al., 2012) (Fig. 6B). It is observed that during most cases of the strong solar activity periods, the AMO was active, the North Atlantic Ocean surface was warm, and the Asian summer monsoon intensity was relatively strong (Fig. 6). However, there are also time periods that solar activity and Asian summer monsoon intensity do not match, e.g., at approximately 5.9, 6.1 and 6.4 ka BP (brown crosses in Fig. 6B). In sum, a compounding impact of the solar activities and the AMO, with AMO playing the most important role, could contribute to the ~60–80-year variability in the Asian summer monsoon.

Numerous studies have shown that the AMV has a significant impact on the inter-decadal variability of the Asian summer monsoon (Duan et al., 2020; Fan et al., 2018; Li et al., 2017; Wang et al., 2022). Its positive/negative phase can affect the Asian monsoon system by modulating the atmospheric tele-connection and air-sea coupling processes. It has been shown that the warm/cold phase of the AMV can stimulate the atmospheric tele-connection wave trains from the Atlantic region eastward to the East Asia-West Pacific region (Si et al., 2021). Through these wave trains, the AMV directly affects the heat transport to Eurasia, increases/decreases the thermal gradients and baroclinic pressure gradients between Eurasia and the neighboring oceans, then enhances/decreases the summer monsoon circulation, and affects the inter-decadal variabilities of the Asian summer monsoon (Si et al., 2021). Besides, the AMV can modulate the inter-decadal variability of the Asian summer monsoon by influencing the large-scale air-sea coupling processes such as the tropical convergence zone in the western Pacific and Indian Oceans, the Hadley Circulation, and the Walker Circulation, which cause anomalies of the SST and circulations in the tropical western Pacific Ocean (Fan et al., 2018). Although the AMV could modulate the Asian summer monsoon through the ENSO variability at the interdecadal timescale (Lu et al., 2006; Zhang et al., 2017), we lack high-resolution ENSO records for comparison during the Mid Holocene (Moy et al., 2002; Rein et al., 2005). Future work on reconstructing high-resolution records of the ENSO, AMV and solar activities is needed to understand the dominant multidecadal mechanisms in modulating the circulation and precipitation in the Asian monsoon region.

5. Conclusions

The precisely $^{230}\text{Th}/\text{U}$ dated, ~4-year-resolution stalagmite $\delta^{18}\text{O}$ and $\delta^{13}\text{C}$ records from Tiechang Cave, Guizhou Province, provides us with a new piece of evidence for interpreting monsoon variations on centennial to decadal timescales in the Mid Holocene. Our sample TC5 sensitively captures the 6.5 ka event, when both $\delta^{18}\text{O}$ and $\delta^{13}\text{C}$ values biased significantly positive from 6.7 to 6.4 ka BP, showing a similar feature as stalagmite records from the Asian monsoon region. Comparing TC5 $\delta^{18}\text{O}$ record with the North Atlantic temperature, NADW and the ice raft debris flux records, we find that the onset of the 6.5 ka event in stalagmite record can be traced back to a cold event centered at 6.8 ka BP that occurred in the subpolar North Atlantic. Increased sea ice coverage weakened the Atlantic horizontal current and perturbed the thermohaline circulation in the eastern Nordic Sea. These perturbations propagated globally, affecting the NADW and causing widespread hemispheric cooling. This further forces the southward movement of the ITCZ, leading to the vegetation degradation in the Africa and the weakening of the Asian monsoon water vapor transport. The 6.5-ka weak monsoon event could also be related to the high ENSO frequency, which caused strengthening in the WPSH and led to enriched rainfall $\delta^{18}\text{O}$. Furthermore, both TC5 $\delta^{18}\text{O}$ and $\delta^{13}\text{C}$ records suggest that the Asian monsoon has sustained multidecadal variability with a dominant cycle of ~60–80 years, possibly reflecting the modulation of the Asian monsoon by multidecadal variability in the Atlantic Ocean and

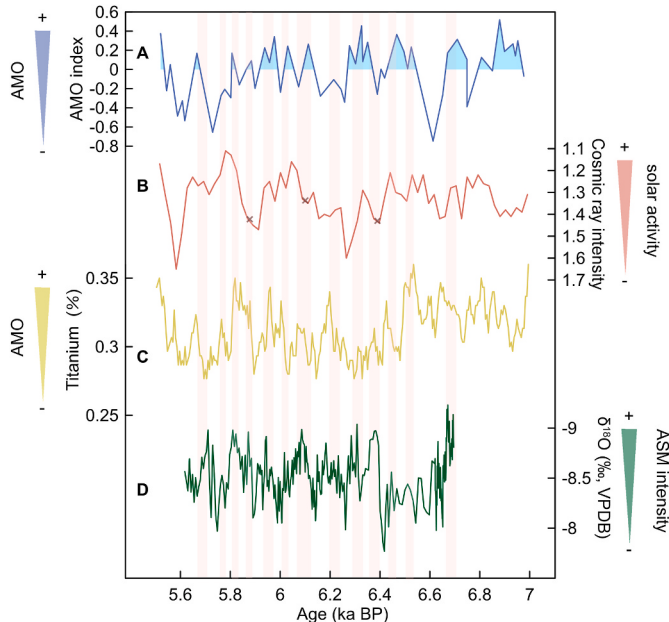


Fig. 6. Causes for the multidecadal Asian summer monsoon variability. (A) The Holocene evolution of the AMO estimated from the KCM HT simulation (Zhang et al., 2016). (B) Cosmic radiation based on the first principal component of several radionuclide records (Steinhilber et al., 2012). (C) Titanium content of sediments in the Cariaco Basin (Haug et al., 2001), which can be used to track the changes in the AMO. (D) $\delta^{18}\text{O}$ record from Tiechang Cave (this study).

the influence of the solar activity. A comparison with AMV index and cosmic ray intensity shows that the AMV should be the main forcing for these ~60–80 years cycles while the solar activity should be a second factor. The AMV, as a characterization of the AMOC, has low-frequency oscillations that modulate the Asian monsoon intensity by influencing the energy balance of the northern hemisphere and altering the interhemispheric temperature gradients.

Author contributions

Bin Zhao: Investigation, Data curation, Writing - Original Draft, Writing- Reviewing and Editing, Funding acquisition. Yingfang Cui: Conceptualization, Writing- Reviewing and Editing, Funding acquisition. Kan Zhao: Data curation, Writing- Reviewing and Editing, Resources, Funding acquisition. Yongjin Wang: Supervision, Writing- Reviewing and Editing, Funding acquisition. Hai Cheng: Data curation. R. Lawrence Edwards: Data curation. Yijia Liang: Conceptualization, Writing- Reviewing and Editing, Funding acquisition.

Declaration of competing interest

The authors declare that they have no known competing financial interests or personal relationships that could have appeared to influence the work reported in this paper.

Acknowledgment

This work was supported by grants from National Key Research and Development Program of China (Grant No. 2023YFF0804700) (Y. Wang), National Natural Science Foundation of China (42207505 (Y. Liang), 41931178 (Y. Wang), 42071105 (K. Zhao)), Jiangsu Province ‘Qinglan Project’ (Y. Cui), the Research and Innovation Team of Nanjing Institute of Tourism and Hospitality (2021KYTD02) (Y. Cui), and the Postgraduate Research & Practice Innovation Program of Jiangsu Province (KYCX25_1982) (B. Zhao).

Appendix A. Supplementary data

Supplementary data to this article can be found online at <https://doi.org/10.1016/j.quascirev.2025.109629>.

Data availability

All data and/or code is contained within the submission.

References

- Ayache, M., Swingedouw, D., Mary, Y., Eynaud, F., Colin, C., 2018. Multi-centennial variability of the AMOC over the Holocene: a new reconstruction based on multiple proxy-derived SST records. *Global Planet. Change* 170, 172–189. <https://doi.org/10.1016/j.gloplacha.2018.08.016>.
- Alley, R., Agustsdóttir, A., 2005. The 8k event: cause and consequences of a major Holocene abrupt climate change. *Quat. Sci. Rev.* 24, 1123–1149. <https://doi.org/10.1016/j.quascirev.2004.12.004>.
- Alley, R.B., Mayewski, P.A., Sowers, T., Stuiver, M., Taylor, K.C., Clark, P.U., 1997. Holocene climatic instability: a prominent, widespread event 8200 yr ago. *Geology* 25, 483. <https://doi.org/10.1130/0091-7613>.
- Axford, Y., Briner, J.P., Miller, G.H., Francis, D.R., 2009. Paleoecological evidence for abrupt cold reversals during peak Holocene warmth on baffin island, arctic Canada. *Quaternary Research* 71, 142–149. <https://doi.org/10.1016/j.yqres.2008.09.006>.
- Baldini, J.U.L., McDermott, F., Baker, A., Baldini, L.M., Matthey, D.P., Railsback, L.B., 2005. Biomass effects on stalagmite growth and isotope ratios: a 20th century analogue from Wiltshire, England. *Earth Planet. Sci. Lett.* 240, 486–494.
- Barber, D.C., Dyke, A., Hillaire-Marcel, C., Jennings, A.E., Andrews, J.T., Kerwin, M.W., Bilodeau, G., McNeely, R., Souton, J., Morehead, M.D., Gagnon, J.-M., 1999. Forcing of the cold event of 8,200 years ago by catastrophic drainage of laurentide lakes. *Nature* 400, 344–348. <https://doi.org/10.1038/22504>.
- Bar-Matthews, M., Ayalon, A., 2011. Mid-Holocene climate variations revealed by high-resolution speleothem records from soreq cave, Israel and their correlation with cultural changes. *Holocene* 21, 163–171. <https://doi.org/10.1177/0959683610384165>.
- Berkelhammer, M., Sinha, A., Stott, L., Cheng, H., Pausata, F.S.R., Yoshimura, K., 2013. An abrupt shift in the indian monsoon 4000 years ago. In: Berkelhammer, L., Fuller, D.Q., Nicoll, K., Flad, R.K., Clift, P.D. (Eds.), *Geophysical Monograph Series*. American Geophysical Union, Washington, D. C., pp. 75–88. <https://doi.org/10.1029/2012GM001207>.
- Bjerknes, J., 1964. Atlantic air-sea interaction. In: *Advances in Geophysics*. Elsevier, pp. 1–82. [https://doi.org/10.1016/S0065-2687\(08\)60005-9](https://doi.org/10.1016/S0065-2687(08)60005-9).
- Bond, G., Kromer, B., Beer, J., Muscheler, R., Evans, M.N., Showers, W., Hoffmann, S., Lotti-Bond, R., Hajdas, I., Bonani, G., 2001. Persistent solar influence on north atlantic climate during the Holocene. *Science* 294, 2130–2136. <https://doi.org/10.1126/science.1065680>.
- Bond, G., Showers, W., Cheseby, M., Lotti, R., Almasi, P., deMenocal, P., Priore, P., Cullen, H., Hajdas, I., Bonani, G., 1997. A pervasive millennial-scale cycle in north atlantic Holocene and glacial climates. *Science* 278, 1257–1266. <https://doi.org/10.1126/science.278.5341.1257>.
- Cai, Y., Cheng, X., Ma, L., Mao, R., Breitenbach, S.F.M., Zhang, H., Xue, G., Cheng, H., Edwards, R.L., An, Z., 2021. Holocene variability of east Asian summer monsoon as viewed from the speleothem $\delta^{18}\text{O}$ records in central china. *Earth Planet. Sci. Lett.* 558, 116758. <https://doi.org/10.1016/j.epsl.2021.116758>.
- Cerling, T.E., 1984. The stable isotopic composition of modern soil carbonate and its relationship to climate. *Earth Planet. Sci. Lett.* 71, 229–240. [https://doi.org/10.1016/0012-821X\(84\)90089-X](https://doi.org/10.1016/0012-821X(84)90089-X).
- Cheng, H., Edwards, R.L., Shen, C.-C., Polyak, V.J., Asmerom, Y., Woodhead, J.D., Hellstrom, J., Wang, Y., Kong, X., Spötl, C., Wang, X., Alexander, E.C., 2013. Improvements in ^{230}Th dating, ^{230}Th and ^{234}U half-life values, and U-Th isotopic measurements by multi-collector inductively coupled plasma mass spectrometry. *Earth Planet. Sci. Lett.* 371, 82–91. <https://doi.org/10.1016/j.epsl.2013.04.006>.
- Consolario, C., Rasmussen, T.L., Panieri, G., 2018. Palaeoceanographic and environmental changes in the eastern fram strait during the last 14,000 years based on benthic and planktonic Foraminifera. *Mar. Micropaleontol.* 139, 84–101. <https://doi.org/10.1016/j.marmicro.2017.11.001>.
- deMenocal, P., Ortiz, J., Guilderson, T., Adkins, J., Sarnthein, M., Baker, L., Yarusinsky, M., 2000. Abrupt onset and termination of the African Humid period: rapid climate responses to gradual insolation forcing. *Quat. Sci. Rev.* 19 (1–5), 347–361. [https://doi.org/10.1016/S0277-3791\(99\)00081-5](https://doi.org/10.1016/S0277-3791(99)00081-5).
- Ding, Y.H., Chan, J.C.L., 2005. The East Asian summer monsoon: an overview. *Meteorol. Atmos. Phys.* 89, 117–142.
- Dixit, Y., Hodell, D.A., Sinha, R., Petrie, C.A., 2014. Abrupt weakening of the indian summer monsoon at 8.2 kyr B.P. *Earth Planet. Sci. Lett.* 391, 16–23. <https://doi.org/10.1016/j.epsl.2014.01.026>.
- Duan, F., Zhang, Z., Wang, Y., Chen, J., Liao, Z., Chen, S., Shao, Q., Zhao, K., 2020. Hydrological variations in central China over the past millennium and their links to the tropical pacific and north atlantic oceans. *Clim. Past* 16, 475–485. <https://doi.org/10.5194/cp-16-475-2020>.
- Edwards, R.L., Chen, J.H., Wasserburg, G.J., 1986. ^{238}U - ^{234}U - ^{230}Th systematics and the precise measurement of time over the past 500,000 years. *Earth Planet. Sci. Lett.* 81, 2–3. [https://doi.org/10.1016/0012-821X\(87\)90154-3](https://doi.org/10.1016/0012-821X(87)90154-3).
- Evan, A., Flamant, C., Gaetani, M., Gaetani, M., Guichard, F., 2016. The past, present and future of African dust. *Nature* 531, 493–495. <https://doi.org/10.1038/nature17149>.
- Fairchild, I.J., Smith, C.L., Baker, A., Fuller, L., Spötl, C., Matthey, D., McDermott, F.E.I.M. F., 2006. Modification and preservation of environmental signals in speleothems. *Earth Sci. Rev.* 75, 105–153. <https://doi.org/10.1016/j.earscirev.2005.08.003>.
- Fan, Y., Fan, K., Xu, Z., Li, S., 2018. ENSO–south China sea summer monsoon interaction modulated by the Atlantic Multidecadal oscillation. *J. Clim.* <https://doi.org/10.1175/JCLI-D-17-0448.1>.
- Fan, H., Hu, Z., Liu, Y., Wang, M., Hu, C., 2024. Holocene variability of the Atlantic multidecadal oscillation and the Pacific decadal oscillation inferred from Chinese speleothem $\delta^{18}\text{O}$ Records. *Paleoceanog and Paleoclimatol* 39. <https://doi.org/10.1029/2023pa004800>.
- Feng, X., Yang, Y., Cheng, H., Zhao, J., Kong, X., Zhang, P., He, Z., Shi, X., Edwards, R.L., 2020. The 7.2 ka climate event: evidence from high-resolution stable isotopes and trace element records of stalagmite in Shuiming Cave, Chongqing, China. *Holocene* 30, 145–154. <https://doi.org/10.1177/0959683619875809>.
- Fleitmann, D., Burns, S.J., Mangini, A., Mudelsee, M., Kramers, J., Villa, I., Neff, U., Al-Subbaray, A.A., Buettner, A., Hippler, D., Matter, A., 2007. Holocene ITCZ and Indian monsoon dynamics recorded in stalagmites from Oman and Yemen (Socotra). *Quaternary Science Reviews* 26 (1–2), 170–188. <https://doi.org/10.1016/j.quascirev.2006.04.012>.
- Fleitmann, D., Burns, S.J., Mudelsee, M., Neff, U., Kramers, J., Mangini, A., Matter, A., 2003. Holocene forcing of the Indian monsoon recorded in a stalagmite from southern Oman. *Science* 300, 1737–1739. <https://doi.org/10.1126/science.1083130>.
- Fohlmeister, J., Voarintsoa, N.R.G., Lechleitner, F.A., Boyd, M., Brandstätter, S., Jacobson, M.J., L. Oster, J., 2020. Main controls on the stable carbon isotope composition of speleothems. *Geochem. Cosmochim. Acta* 279, 67–87. <https://doi.org/10.1016/j.gca.2020.03.042>.
- Genty, D., Genty, D., Blamart, D., Ouahdi, R., Gilmour, M., Baker, A., Jouzel, J., Jouzel, J., Jouzel, J., Jouzel, Jean, Van-Exter, S., 2003. Precise dating of Dansgaard-Oeschger climate oscillations in western Europe from stalagmite data. *Nature* 421, 833–837. <https://doi.org/10.1038/nature01391>.
- Gleissberg, W., 1965. The eighty-year solar cycle in auroral frequency numbers. *J. Br. Astron. Assoc.* 75, 227–231.
- Griffiths, M.L., Johnson, K.R., Pausata, F.S.R., White, J.C., Henderson, G.M., Wood, C.T., Yang, H., Ersek, V., Conrad, C., Sekhon, N., 2020. End of green Sahara amplified mid- to late Holocene megadroughts in mainland Southeast Asia. *Nat. Commun.* 11, 4204. <https://doi.org/10.1038/s41467-020-17927-6>.

- Grinsted, A., Moore, J.C., Jevrejeva, S., 2004. Application of the cross wavelet transform and wavelet coherence to geophysical time series. *Nonlinear Processes in Geophysics* 11, 561–566.
- Haug, G.H., Hughen, K.A., Sigman, D.M., Peterson, L.C., Röhl, U., 2001. Southward migration of the intertropical convergence zone through the Holocene. *Science* 293, 1304–1308. <https://doi.org/10.1126/science.1059725>.
- Hoogakker, B.A.A., Chapman, M.R., McCave, I.N., Hillaire-Marcel, C., Ellison, C.R.W., Hall, I.R., Telford, R.J., 2011. Dynamics of North Atlantic deep water masses during the Holocene. *Paleoceanography* 26. <https://doi.org/10.1029/2011PA002155>, 2011PA002155.
- Hou, J., Huang, Y., Shuman, B.N., Oswald, W.W., Foster, D.R., 2012. Abrupt cooling repeatedly punctuated early-holocene climate in eastern North America. *Holocene* 22, 525–529. <https://doi.org/10.1177/0959683611427329>.
- Hu, C., Henderson, G.M., Huang, J., Xie, S., Sun, Y., Johnson, K.R., 2008. Quantification of Holocene Asian monsoon rainfall from spatially separated cave records. *Earth Planet Sci. Lett.* 266, 221–232. <https://doi.org/10.1016/j.epsl.2007.10.015>.
- Isono, D., Yamamoto, M., Irino, T., Oba, T., Murayama, M., Nakamura, T., Kawahata, H., 2009. The 1500-year climate oscillation in the midlatitude north pacific during the Holocene. *Geology* 37 (1), 591–594. <https://doi.org/10.1130/G25667A>.
- Jaffey, A.H., Flynn, K.F., Glendenin, L.E., Bentley, W.C., Essling, A.M., 1971. Precision measurement of half-lives and specific activities of U235 and U238. *Phys. Rev. C* 4, 1889–1906. <https://doi.org/10.1103/PhysRevC.4.1889>.
- Jo, K., Yi, S., Lee, J.-Y., Woo, K.S., Cheng, H., Edwards, L.R., Kim, S.-T., 2017. 1000-year quasi-periodicity of weak monsoon events in temperate northeast Asia since the mid-Holocene. *Sci. Rep.* 7, 15196. <https://doi.org/10.1038/s41598-017-15566-4>.
- Johnsen, S.J., Dahl-Jensen, D., Gundestrup, N., Steffensen, J.P., Clausen, H.B., Miller, H., Masson-Delmotte, V., Sveinbjörnsdóttir, A.E., White, J., 2001. Oxygen isotope and paleaeotemperature records from six Greenland ice-core stations: camp Century, Dye-3, GRIP, GISP2, Renland and NorthGRIP. *J. Quat. Sci.* 16, 299–307. <https://doi.org/10.1002/jqs.622>.
- Knudsen, M.F., Seidenkrantz, M.-S., Jacobsen, B.H., Kuijpers, A., 2011. Tracking the Atlantic Multidecadal oscillation through the last 8,000 years. *Nat. Commun.* 2. <https://doi.org/10.1038/ncomms1186>.
- Lechleitner, F.A., Day, C.C., Kost, O., Wilhelm, M., Haghipour, N., Henderson, G.M., Stoll, H.M., 2021. Stalagmite carbon isotopes suggest deglacial increase in soil respiration in western Europe driven by temperature change. *Clim. Past* 17, 1903–1918. <https://doi.org/10.5194/cp-17-1903-2021>.
- Li, S., Wu, L., Wang, Y., Geng, T., Cai, W., Gan, B., Jing, Z., Yang, Y., 2025. Intensified atlantic multidecadal variability in a warming climate. *Nat. Clim. Change* 15, 293–300. <https://doi.org/10.1038/s41558-025-02252-x>.
- Li, Y., Ding, Y., Li, W., 2017. Interdecadal variability of the Afro-Asian summer monsoon system. *Adv. Atmos. Sci.* 34, 833–846. <https://doi.org/10.1007/s00376-017-6247-7>.
- Liang, Y., Zhao, K., Wang, Y., Edwards, R.L., Cheng, H., Shao, Q., Chen, S., Wang, J., Zhu, J., 2022. Different response of stalagmite d18O and d13C to millennial-scale events during the last glacial, evidenced from Huangjin Cave, northern China. *Quat. Sci. Rev.* 14.
- Liang, Y., Zhang, Z., Li, J., Zhao, B., Wang, Q., Wang, Y., Cheng, H., 2024. Multidecadal monsoon variations during the early last deglaciation revealed by speleothem record from southwestern China. *Minerals* 14, 346. <https://doi.org/10.3390/min1404346>.
- Liu, W., Fedorov, A.V., Xie, S.-P., Hu, S., 2020. Climate impacts of a weakened Atlantic meridional overturning circulation in a warming climate. *Sci. Adv.* 6, eaaz4876. <https://doi.org/10.1126/sciadv.aaz4876>.
- Liu, D., Wang, Y., Cheng, H., Edwards, R.L., Kong, X., 2015. Cyclic changes of Asian monsoon intensity during the early mid-Holocene from annually-laminated stalagmites, central China. *Quaternary Science Reviews* 121, 1–10. <https://doi.org/10.1016/j.quascirev.2015.05.003>.
- Liu, W., Xie, S.-P., Liu, Z., Zhu, J., 2017. Overlooked possibility of a collapsed atlantic meridional overturning circulation in warming climate. *Sci. Adv.* 3, e1601666. <https://doi.org/10.1126/sciadv.1601666>.
- Lu, F., Lu, H., Gu, Y., Lin, P., Lu, Z., Zhang, Q., Zhang, H., Yang, F., Dong, X., Yi, S., Chen, D., Pausata, F.S.R., Ben-Yami, M., Mecking, J.V., 2025. Tipping point-induced abrupt shifts in east Asian hydroclimate since the last glacial maximum. *Nat. Commun.* 16, 477. <https://doi.org/10.1038/s41467-025-55888-w>.
- Lu, R., Dong, B., Ding, H., 2006. Impact of the Atlantic Multidecadal oscillation on the Asian summer monsoon. *Geophys. Res. Lett.* 33, 2006GL027655. <https://doi.org/10.1029/2006GL027655>.
- Mayewski, P.A., Rohling, E.E., Curt Stager, J., Karlén, W., Maasch, K.A., Meeker, L.D., Meyerson, E.A., Gasse, F., Van Kreveld, S., Holmgren, K., Lee-Thorp, J., Rosqvist, G., Rack, F., Staubwasser, M., Schneider, R.R., Steig, E.J., 2004. Holocene climate variability. *Quaternary Research* 62, 243–255. <https://doi.org/10.1016/j.yqres.2004.07.001>.
- McDermott, F., 2004. Palaeo-climate reconstruction from stable isotope variations in speleothems: a review. *Quat. Sci. Rev.* 23, 901–918. <https://doi.org/10.1016/j.quascirev.2003.06.021>.
- McKay, N.P., Kaufman, D.S., Arcusa, S.H., Kulus, H.R., Edge, D.C., Erb, M.P., Hancock, C. L., Routson, C.C., Żarczyński, M., Marshall, L.P., Roberts, G.K., Telles, F., 2024. The 4.2 ka event is not remarkable in the context of Holocene climate variability. *Nat. Commun.* 15, 6555. <https://doi.org/10.1038/s41467-024-50886-w>.
- Moros, M., Andrews, J.T., Eberl, D.D., Jansen, E., 2006. Holocene history of drift ice in the northern north atlantic: evidence for different spatial and temporal modes. *Paleoceanography* 21, 2005PA001214. <https://doi.org/10.1029/2005PA001214>.
- Moy, C., Seltzer, G., Rodbell, D., et al., 2002. Variability of El Niño/Southern Oscillation activity at millennial timescales during the Holocene epoch. *Nature* 420, 162–165. <https://doi.org/10.1038/nature01194>.
- Owen, R.A., Day, C.C., Hu, C.-Y., Liu, Y.-H., Pointing, M.D., Blättler, C.L., Henderson, G. M., 2016. Calcium isotopes in caves as a proxy for aridity: modern calibration and application to the 8.2 kyr event. *Earth Planet Sci. Lett.* 443, 129–138. <https://doi.org/10.1016/j.epsl.2016.03.027>.
- Peristykh, A.N., Damon, P.E., 2003. Persistence of the Gleissberg 88-year solar cycle over the last ~12,000 years: evidence from cosmogenic isotopes. *J. Geophys. Res.* 108. <https://doi.org/10.1029/2002ja009390>.
- Rein, B., Lückge, A., Reinhardt, L., Sirocko, F., Wolf, A., Dullo, W., 2005. El Niño variability off Peru during the last 20,000 years. *Paleoceanography* 20. <https://doi.org/10.1029/2004pa001099>.
- Ren, W., Yi, G., 2019. Characteristics of time-transgressive Holocene optimum in the east Asian monsoon region. *Earth Sci. Res.* 23, 259–263. <https://doi.org/10.15446/esrj.v23n3.72188>.
- Schlesinger, M.E., Ramankutty, N., 1994. An oscillation in the global climate system of period 65–70 years. *Nature* 367, 723–726. <https://doi.org/10.1038/367723a0>.
- Shen, C.-C., Edwards, R.L., Cheng, H., Dorale, J.A., Thomas, R.B., Moran, S.B., Moran, S., Bradley, Weinstein, S.E., Edmonds, H.N., 2002. Uranium and thorium isotopic and concentration measurements by magnetic sector inductively coupled plasma mass spectrometry. *Chem. Geol.* 185, 165–178. [https://doi.org/10.1016/s0009-2541\(01\)00404-1](https://doi.org/10.1016/s0009-2541(01)00404-1).
- Si, D., Jiang, D., Ding, Y., 2021. Synergistic impacts of the atlantic and pacific oceans on interdecadal variations of summer rainfall in northeast Asia. *Journal of Meteorological Research* 35, 844–856. <https://doi.org/10.1007/s13351-021-0191-2>.
- Steinhilber, F., Abreu, J.A., Beer, J., Brunner, I., Christl, M., Fischer, H., Heikkilä, U., Kubik, P.W., Mann, M., McCracken, K.G., Miller, H., Miyahara, H., Oerter, H., Wilhelms, F., 2012. 9,400 years of cosmic radiation and solar activity from ice cores and tree rings. *Proc Natl Acad Sci USA* 109, 5967–5971. <https://doi.org/10.1073/pnas.1118965109>.
- Sun, Y., Clemens, S.C., Morrill, C., Lin, X., Wang, X., An, Z., 2012. Influence of Atlantic meridional overturning circulation on the East Asian winter monsoon. *Nat. Geosci.* 5, 46–49. <https://doi.org/10.1038/ngeo1326>.
- Tan, L., Li, Y., Wang, X., Cai, Y., Lin, F., Cheng, H., Ma, L., Sinha, A., Edwards, R.L., 2020. Holocene monsoon change and abrupt events on the western chinese Loess plateau as revealed by accurately dated stalagmites. *Geophys. Res. Lett.* 47, e2020GL090273. <https://doi.org/10.1029/2020GL090273>.
- Tan, M., 2014. Circulation effect: response of precipitation δ18O to the ENSO cycle in monsoon regions of China. *Clim. Dyn.* 42, 1067–1077. <https://doi.org/10.1007/s00382-013-1732-x>.
- Telesiński, M.M., Bauch, H.A., Spielhagen, R.F., Kandiano, E.S., 2015. Evolution of the central Nordi Seas over the last 20 thousand years. *Quat. Sci. Rev.* 121, 98–109. <https://doi.org/10.1016/j.quascirev.2015.05.013>.
- Telesiński, M.M., Liu, W., Ren, X., Zajączkowski, M., 2024. Worldwide consequences of a mid-holocene cold event in the Nordic Seas. *Quat. Sci. Rev.* 344, 109002. <https://doi.org/10.1016/j.quascirev.2024.109002>.
- Viau, A.E., Gajewski, K., Sawada, M.C., Fines, P., 2006. Millennial-scale temperature variations in North America during the Holocene. *J. Geophys. Res. Atmos.* 111, 2005JD006031. <https://doi.org/10.1029/2005JD006031>.
- Wang, K., Zhao, J., Wang, J., Li, H., Nie, J., Liu, J., Shi, Z., Li, Y., Lu, J., Cheng, H., 2025. Past decadal climate variability of east Asian summer monsoon: characteristics and mechanisms. *Science Bulletin* 70, 240–261. <https://doi.org/10.1360/TB-2024-0161>.
- Wang, M., Hu, C., Liu, Y., Li, L., Xie, S., Johnson, K., 2022. Precipitation in eastern China over the past millennium varied with large-scale climate patterns. *Commun. Earth Environ.* 3 (1), 321. <https://doi.org/10.1038/s43247-022-00664-7>.
- Wang, N., Dee, S., Hu, J., Steiger, N., Thirumalai, K., 2024. PDO and AMO modulation of the ENSO–Asian summer monsoon teleconnection during the last millennium. *JGR Atmospheres* 129. <https://doi.org/10.1029/2023jd039638>.
- Wang, Y., Cheng, H., Edwards, R.L., He, Y., Kong, X., An, Z., Wu, J., Kelly, M.J., Dykoski, C.A., Li, X., 2005. The Holocene Asian monsoon: links to solar changes and north Atlantic climate. *Science* 308, 854–857. <https://doi.org/10.1126/science.1106296>.
- Wang, Z., Chen, S., Wang, Y., Cheng, H., Liang, Y., Yang, S., Zhang, Z., Zhou, X., Wang, M., 2020. Sixty-year quasi-period of the Asian monsoon around the last interglacial derived from an annually resolved stalagmite δ18O record. *Palaeogeogr. Palaeoclimatol. Palaeoecol.* 541, 109545. <https://doi.org/10.1016/j.palaeo.2019.109545>.
- Wanner, H., Solomina, O., Grosjean, M., Ritz, S.P., Jetel, M., 2011. Structure and origin of Holocene cold events. *Quat. Sci. Rev.* 30, 3109–3123. <https://doi.org/10.1016/j.quascirev.2011.07.010>.
- Werner, K., Spielhagen, R.F., Bauch, D., Hass, H.C., Kandiano, E., 2013. Atlantic water advection versus sea-ice advances in the eastern strait during the last 9 ka: multiproxy evidence for a two-phase Holocene. *Paleoceanography* 28, 283–295. <https://doi.org/10.1002/palo.20028>.
- Wu, J., Shen, C., Yang, H., Qian, S., Xie, S., 2023. Holocene temperature variability in China. *Quat. Sci. Rev.* 312, 108184. <https://doi.org/10.1016/j.quascirev.2023.108184>.
- Xiao, J., Chang, Z., Wen, R., Zhai, D., Itoh, S., Lomtatidze, Z., 2009. Holocene weak monsoon intervals indicated by low lake levels at hulun lake in the monsoonal margin region of northeastern inner Mongolia, China. *Holocene* 19, 899–908. <https://doi.org/10.1177/0959683609336574>.
- Zhang, R., Min, Q., Su, J., 2017. Impact of El Niño on atmospheric circulations over east Asia and rainfall in China: role of the anomalous western North Pacific anticyclone. *Sci. China Earth Sci.* 60, 1124–1132. <https://doi.org/10.1007/s11430-016-9026-x>.
- Zhang, Z., Leduc, G., Sachs, J. P., 2014. El Niño evolution during the Holocene revealed by a biomarker rain gauge in the Galápagos Islands. *Earth and Planetary Science Letters* 404, 420–434. <https://doi.org/10.1016/j.epsl.2014.07.013>.

- Zhang, Z., Liu, J., Chen, J., Chen, S., Shen, Z., Chen, J., Liu, X., Wu, D., Sheng, Y., Chen, F., 2021. Holocene climatic optimum in the east Asian monsoon region of China defined by climatic stability. *Earth Sci. Rev.* 212, 103450. <https://doi.org/10.1016/j.earscirev.2020.103450>.
- Zhang, H., Pu, X., 2011. Stalagmite records of climate change and cold—dry events during the middle Holocene in Xundian, Yunnan. *Acta Geoscientica Sinica* 32 (1), 6. <https://doi.org/10.3975/cagssb.2011.01.12> (in Chinese with English Abstract).
- Zhang, M., Tu, I., Lin, Y., Qin, J., Wang, H., Feng, Y., Yang, Y., Zhu, X., 2004. The cooling events from stalagmite records during the middle and late Holocene in Southwest China. *Carsol. Sin./Zhong Guo Yan Rong* 23 (4), 7. <https://doi.org/10.3969/j.issn.1001-4810.2004.04.005> (in Chinese with English Abstract).
- Zhang, N., Yang, Y., Cheng, H., Zhao, J., Yang, X., Liang, S., Nie, X., Zhang, Y., Edwards, R.L., 2018. Timing and duration of the East Asian summer monsoon maximum during the Holocene based on stalagmite data from North China. *Holocene* 28, 1631–1641. <https://doi.org/10.1177/0959683618782606>.
- Zhang, X., Jin, L., Jia, W., 2016. Centennial-scale teleconnection between North Atlantic sea surface temperatures and the Indian summer monsoon during the Holocene. *Clim. Dyn.* 46, 3323–3336. <https://doi.org/10.1007/s00382-015-2771-2>.
- Zhao, C., Rohling, E.J., Liu, Zhengyu, Yang, Xiaoqiang, Zhang, E., Cheng, J., Liu, Zhonghui, An, Z., Yang, Xiangdong, Feng, X., Sun, X., Zhang, C., Yan, T., Long, H., Yan, H., Yu, Z., Liu, W., Yu, S.-Y., Shen, J., 2021. Possible obliquity-forced warmth in southern Asia during the last glacial stage. *Science Bulletin* 66, 1136–1145. <https://doi.org/10.1016/j.scib.2020.11.016>.
- Zhao, K., Wang, Y., Edwards, R.L., Cheng, H., Liu, D., Kong, X., Ning, Y., 2016. Contribution of ENSO variability to the East Asian summer monsoon in the late Holocene. *Palaeogeogr. Palaeoclimatol. Palaeoecol.* 449, 510–519. <https://doi.org/10.1016/j.palaeo.2016.02.044>.